



**Hemodynamic differences between recurrent and non-recurrent intracranial aneurysms: fluid dynamics simulations based on MR angiography**

Journal:	<i>Journal of Neuroimaging</i>
Manuscript ID	JON-18-5353.R2
Wiley - Manuscript type:	Experimental Laboratory Research
Date Submitted by the Author:	n/a
Complete List of Authors:	Schönfeld, Michael; Universitätsklinikum Hamburg-Eppendorf, Department of Diagnostic and Interventional Neuroradiology Forkert, Nils Daniel; University of Calgary Cumming School of Medicine, Department of Radiology & Hotchkiss Brain Institute Fiehler, Jens Cho, Young Dae Han, Moon Hee ; National University Hospital, Department of Radiology, Seoul Kang, Hyun-Seung; Seoul National University Hospital, Neurosurgery Peach, Thomas Byrne, James
Keywords:	aneurysm, computational fluid dynamics, endovascular, intracranial, hemodynamics
Subject Area:	MR Angiography (MRA) < Magnetic Resonance (MR) < Imaging Techniques < NEUROIMAGING

SCHOLARONE™  
Manuscripts

# Hemodynamic differences between recurrent and non-recurrent intracranial aneurysms: fluid dynamics simulations based on MR angiography

Authors: Michael Hinrich Schönfeld<sup>1</sup>, Nils Daniel Forkert<sup>2</sup>, Jens Fiehler<sup>1</sup>, Young Dae Cho<sup>3</sup>, Moon Hee Han<sup>3</sup>, Hyun-Seung Kang<sup>4</sup>, Thomas William Peach<sup>5,6</sup>, James Vincent Byrne<sup>7</sup>.

<sup>1</sup>Department of Diagnostic and Interventional Neuroradiology, University Medical Center Hamburg-Eppendorf, Hamburg, Germany.

<sup>2</sup>Department of Radiology and Hotchkiss Brain Institute, University of Calgary, Calgary, Canada.

<sup>3</sup>Department of Radiology, Seoul National University Hospital, Seoul National University College of Medicine, Seoul, Korea

<sup>4</sup>Department of Neurosurgery, Seoul National University Hospital, Seoul National University College of Medicine, Seoul, Korea

<sup>5</sup>Department of Mechanical Engineering, University College London, London, UK

<sup>6</sup>Institute of Biomedical Engineering, Department of Engineering Science, University of Oxford, Oxford, UK

<sup>7</sup>Oxford Neurovascular & Neuroradiology Research Unit, Oxford Radcliffe Hospital, Oxford, UK

**Running title:** CFD based on 3D-TOF-MRA in aneurysm recurrence

**Keywords:** aneurysm, computational fluid dynamics, endovascular, intracranial, hemodynamics

## Corresponding Author:

Michael H. Schönfeld, MD  
Department of Diagnostic and Interventional Neuroradiology  
University Medical Center Hamburg-Eppendorf  
Martinistr. 52 20246 Hamburg, Germany  
[m.schoenfeld@uke.de](mailto:m.schoenfeld@uke.de)

**Acknowledgements and Disclosures:** The authors acknowledge the use of the Oxford Advanced Research Computing (ARC) facility in carrying out this work and would like to thank Prof. Y Ventikos, and both Dr M. Megahed and the ESI Group for allowing the use of the CFD-ACE suite.

This research received no specific grant from any funding agency in the public, commercial, or not-for-profit sectors.

The authors declare that they have no conflict of interest.

**Abstract:****Background and Purpose:**

Whereas the role of wall shear stress (WSS) in the initiation, growth, and rupture of intracranial aneurysms has been well studied, its influence on aneurysm recurrence after endovascular treatment requires further investigation. We aimed to compare WSS at necks of recurrent and non-recurrent aneurysms.

**Methods:**

Nine recurrent coil-embolized aneurysms were identified and matched with nine non-recurrent aneurysms. Patient-specific vessel geometries reconstructed from follow-up 3D time-of-flight magnetic resonance angiography were analyzed using computational fluid dynamics (CFD) simulations. Absolute WSS and the percentage of abnormally low and high WSS at the aneurysm neck compared to the near artery were measured.

**Results:**

The median percentage of abnormal WSS at the aneurysm neck was 49.3% for recurrent and 34.7% for non-recurrent aneurysms ( $p = 0.011$ ). The area under the receiver-operating-characteristic curve for distinguishing these aneurysms according to the percentage of abnormal WSS was 0.86 (95% CI 0.62 to 0.98). The optimal cut-off value of 45.1% resulted in a sensitivity and a specificity of 88.89% (95% CI 51.8 – 99.7%).

**Conclusion:**

Our findings indicate that necks of recurrent aneurysms are exposed to abnormal WSS to a larger extent. Abnormal WSS may serve as a metric to distinguish them from non-recurrent aneurysms with CFD simulations a priori.

## Introduction:

Hemodynamic forces play an important role in the initiation, growth and rupture of untreated aneurysms.<sup>1-5</sup> Additionally, they seem to be able to predict worsening of aneurysm occlusion after endovascular treatment in certain locations.<sup>6</sup>

Few studies have been published in which aneurysm recurrences were examined with computational fluid dynamics (CFD) models.<sup>6-10</sup> Most studies use vascular models derived from 3D-rotational angiography (3D-RA) since it provides the highest resolution and allows segmentation of vessel with high accuracy.<sup>11</sup> Although routinely used for diagnosis and treatment planning of cerebral aneurysms, 3D-RA is not commonly used as the first-line modality for follow-up imaging. 3D time-of-flight magnetic resonance angiography (3D-TOF-MRA), on the other hand, is generally employed for follow-up imaging of coiled aneurysms<sup>12</sup> because of its low invasiveness compared to 3D-RA, digital subtraction angiography (DSA), and contrast enhanced MRA.<sup>13</sup> Recently, the feasibility of CFD analysis based on 3D-TOF-MRA follow-up imaging has been demonstrated in a study that found hemodynamic vascular biomarkers for aneurysm initiation.<sup>5</sup>

The aim of this study is to analyze hemodynamic factors at the aneurysm neck that may influence recurrence. We hypothesize that CFD modelling using 3D TOF-MRA data can identify putative hemodynamic conditions for recurrence development after coil embolisation.

## Material and Methods:

### *Patients and aneurysms*

The datasets used in this study were collected within the context of a prospective multi-center observational study<sup>14</sup> and in a retrospective fashion from an interventional neuroradiological database from a single institution. Ethical approval was granted by the institutional review board. Patients with ruptured or unruptured aneurysms that were treated with coil embolisation were consecutively registered from July 2008

1 to July 2009 and imaging outcomes were assessed by an independent core laboratory. The criteria for patient  
2 inclusion and exclusion as well as the standardized treatment protocol have been described in previous  
3 studies.<sup>14,15</sup>  
4  
5  
6  
7

### 8 *Follow up imaging and recurrence definition*

9

10 Follow-up imaging protocols included MR angiography at 6 months (6FU) and 1 year (12FU). 3D-TOF-  
11 MRA imaging was performed at both time points without application of contrast agent on 1.5T MRI  
12 scanners with the following imaging parameters: TE = 6.9ms, TR = 25ms, flip angle = 20°, image in-plane  
13 resolution = 0.21 mm<sup>2</sup>, and slice thickness = 0.5 mm.  
14  
15  
16  
17  
18  
19

20 Recurrences between 6FU and 12FU in the cohort were identified in a previous study by the means of  
21 volumetric measurements (33 recurrences in 297 aneurysms).<sup>16</sup> As pretesting of sample geometries  
22 suggested that internal cerebral artery (ICA) geometries were subject to a high rate of non-convergence only  
23 non-ICA geometries were included. Cases with inconclusive results regarding the presence or absence of a  
24 recurrence in the volumetric measurements were excluded. Recurrences that could be visually identified on  
25 3D-TOF-MRA were verified with digital subtraction angiography.  
26  
27  
28  
29  
30  
31  
32  
33  
34

### 35 *Matching of patients*

36

37 Recurrent and non-recurrent aneurysms were initially sorted and then matched in the following order: 1. by  
38 exact aneurysm location, 2. by nearest neck width, 3. by nearest pre-interventional aneurysm volume, and 4.  
39 by nearest packing density.  
40  
41  
42  
43  
44  
45  
46  
47  
48  
49  
50  
51  
52  
53  
54  
55  
56  
57  
58  
59  
60

## *Computational fluid dynamic simulation of patient specific geometries*

Since patient specific flow information were not available for the present study, population averaged flow conditions of the internal cerebral artery, middle cerebral artery, and vertebral artery as described in the literature were used to model parabolic inlet profiles.<sup>17</sup> The flow rates in the anterior cerebral artery and basilar artery were calculated by subtracting the middle cerebral artery flow from the internal cerebral artery flow and doubling the vertebral artery flow rate, respectively.

Patient-specific vascular models of the selected aneurysms were reconstructed from 3D TOF-MRA datasets acquired at 6 months after treatment. In a first step, the vascular geometry including the parent vessel, the aneurysm neck, and the first branching vessels was extracted as a triangular surface mesh from the source 3D TOF-MRA data using GIMIAS (Graphical Interface for Medical Image Analysis and Simulation; Center for Computational Imaging and Simulation Technologies in Biomedicine, Universitat Pompeu Fabra, Barcelona, Spain).

Therefore, the vascular structure of interest was semi-automatically segmented using global thresholding within the selected volume-of-interest. The threshold needed for this was visually selected aiming to segment all arterial structures but excluding any non-vascular structures. Next, the marching cubes algorithm was applied to generate a surface mesh of the vessel geometry based on the segmented vessel structures. The surface mesh was then smoothed using a non-shrinking algorithm with 100 iterations. Planar openings of the surface models were generated by trimming the straight segments of the inlet vessel and the outlet vessels perpendicular to their axes on the smoothed models within ten vessel diameters upstream and downstream of the aneurysm location for prescribing the boundary conditions. Lastly, a loop subdivision filter was applied to globally refine the mesh by increasing the number of triangles in the mesh. Quality of the geometries in reference to the source data and maximum intensity projections of the 3D TOF-MRA datasets was confirmed by a neuroradiologist (MHS) and a CFD engineer (TWP).

1 Each vessel geometry was imported into Blender (Stichting Blender Foundation, Amsterdam, Netherlands)  
2 to measure the diameters and the area of the vessel inlet. The aneurysm geometries were imported into CFD-  
3 VisCART (ESI Group, Paris, France) for meshing. The meshing of each geometry was completed with a  
4 Projected Single Domain mesh, an Omnitree Cartesian tree type, and three near-wall Cartesian layers to give  
5 a smooth and well-resolved boundary definition. All the simulations were run on meshes with a minimum  
6 mesh density of 8000 elements/mm<sup>3</sup>, resulting in mesh sizes between 1.9 and 4.0 million elements and  
7 assuming mesh independence as per previous studies.<sup>18</sup> To reduce the computation time, a steady-state,  
8 radially symmetric parabolic velocity profile was prescribed at the inlet of each aneurysm geometry as  
9 steady-state flow simulations of the cerebral vasculature have been reported to be just as effective as  
10 pulsatile flow simulations for estimating most key indices.<sup>19</sup> A flow rate typical of the mean flow rate of  
11 each vessel type (internal carotid artery = 216 ml/min; middle cerebral artery = 150ml/min; anterior cerebral  
12 artery = 66 ml/min; basilar artery = 144 ml/min) was used as an inlet boundary condition and a constant  
13 pressure condition was imposed at all outlet vessels. Where this outlet condition was applied to more than  
14 one daughter vessel the corresponding outlet flow split each was compared to population average values  
15 with no substantial departure seen in each daughter vessel.<sup>20</sup> The average diameters at the vessel inlets  
16 across the geometries was 3.1mm with a corresponding average blood velocity of 0.34 m/s. Because of the  
17 small vessel diameters and low blood flow velocity, the resultant low Reynolds number in the simulated  
18 vasculature (177 to 315) confirmed the laminar nature of the flow.

19 Blood was assumed incompressible and Newtonian with a density of 1060kg/m<sup>3</sup> and a dynamic viscosity of  
20 0.0035 Pa·s. A rigid arterial wall was assumed for computational efficiency, which has been shown to have  
21 little effect on the flow patterns seen when compared to simulations with elastic compliant walls.<sup>21</sup> The  
22 steady-state Navier-Stokes equation was solved using the finite-volume method in the Multiphysics suite  
23 CFD-ACE GUI (ESI Group, Paris, France) utilizing a central differencing scheme for spatial differencing,  
24 along with SIMPLE-Consistent (SIMPLEC) pressure correction and an algebraic multi-grid method for  
25 convergence acceleration.

1 Simulations were run in the University of Oxford Advance Research Computing facility<sup>22</sup> on 16 2.93GHz  
2 cores and each simulation was found to typically converge to five orders of magnitude residual reduction in  
3 500 to 1000 iterations.  
4  
5

### 6 *Quantitative evaluation*

7  
8 To calculate hemodynamic indices in CFD-VIEW (ESI Group, Paris, France), the aneurysm necks were  
9  
10 isolated from the contiguous vasculature using cutting planes in the first step. The adjacent vasculature at a  
11 distance of up to 1 cm from the aneurysm neck was defined as the near vessel, as previously proposed by  
12  
13 Cebal et al.<sup>3</sup> The maximum, mean, and median values of simulated WSS together with the standard  
14  
15 deviation (SD) in the near vessel and the aneurysm neck were calculated for all cases using Matlab (Version  
16  
17 R2014a.; The MathWorks Inc., Natick, Massachusetts, USA).  
18  
19

20  
21 In addition to the measurement of the maximal and space-averaged WSS, the WSS was also normalized by  
22  
23 the average near vessel WSS value to become a non-dimensional number to minimize the dependence on  
24  
25 inlet conditions as suggested before.<sup>1</sup>  
26  
27

28  
29 We calculated the percentage of the area at the aneurysm neck that is exposed to abnormal WSS as the  
30  
31 percentage area with either abnormally low or abnormally high WSS. Some definitions for abnormal WSS  
32  
33 require parametric statistical estimates such as mean and SD, although in many cases WSS in the near-vessel  
34  
35 region is not normally distributed. As proposed by Retarekar et al.,<sup>19</sup> we defined a WSS at the aneurysms  
36  
37 neck to be “abnormally” high or low if it was higher than the 84.13<sup>th</sup> percentile or lower than the 15.87<sup>th</sup>  
38  
39 percentile of the WSS of the near artery (the non-parametric equivalent of mean $\pm$  SD in a normal  
40  
41 distribution). Where the WSS distribution is indeed normally distributed this definition leads to the same  
42  
43 results as the definition employed by Cebal et al.<sup>3</sup>  
44  
45  
46  
47  
48  
49  
50  
51

### 52 *Qualitative evaluation*

53  
54 Models of the vessel geometries with WSS magnitude distribution plotted at the vessel wall (color scaled to  
55  
56 a minimum WSS of 0 Pa and a maximum WSS of 20 Pa) were visualized in CFD-VIEW. Flow patterns in  
57  
58 the vasculature were visualized with instantaneous streamlines colored according to the flow velocity  
59  
60

1 magnitude (color scaled to a minimum velocity of  $0 \text{ m}\cdot\text{s}^{-1}$  and a maximum velocity of  $0.5 \text{ m}\cdot\text{s}^{-1}$ ). These  
2 models were evaluated for patterns that were discriminative between aneurysms that exhibited a recurrence  
3 and those that did not. Figure 1 illustrates the methods of qualitative and quantitative evaluation on the  
4 example of a non-recurrent middle cerebral artery aneurysm.  
5  
6  
7  
8  
9

### 10 *Statistical analysis*

11  
12 Data were expressed as mean  $\pm$  SD or median with the interquartile range as appropriate. For qualitative  
13 data, the chi-square test was used to compare the differences between the two groups. For quantitative data,  
14 the Shapiro-Wilk test was used to test for normality and an independent-samples t-test or u-test was used as  
15 appropriate. A receiver operating characteristics (ROC)-curve analysis was performed to calculate the area  
16 under the ROC curve (AUC) and determine the optimal threshold value for the percentage of abnormal WSS  
17 area that discriminates recurrent from non-recurrent aneurysms using Youden's index. A p value of  $< 0.05$   
18 was regarded as statistically significant. Statistical analysis was performed with SPSS 19.0 package (IBM  
19 SPSS Statistics for Windows, Armonk, NY, USA), while the ROC-curve analysis was performed with  
20 MedCal (MedCal Software, Ostend, Belgium).  
21  
22  
23  
24  
25  
26  
27  
28  
29  
30  
31  
32  
33  
34  
35  
36  
37

## 38 **Results:**

### 39 *Study population*

40  
41  
42 13 cases of recurrent aneurysms met the inclusion criteria, but 4 aneurysms had to be excluded because (1)  
43 no matching geometry could be found in the cohort of non-recurred aneurysms for two aneurysms, (2)  
44 artefacts from a stent in the parent vessel did not allow for an accurate vessel geometry in one aneurysm and  
45 (3) steady-state flow simulation did not reach convergence in one aneurysm.  
46  
47  
48  
49  
50  
51  
52  
53

54 The remaining nine datasets of recurrent aneurysms were matched to nine aneurysms selected from the non-  
55 recurrent cohort. Both groups consisted of six MCA aneurysms, two BA termination aneurysms, and one  
56 anterior communication artery (ACom) aneurysm each. All 18 aneurysms were rated to be 90% or 95%  
57  
58  
59  
60

1 occluded as assessed on the post-interventional DSA runs. No significant difference was found between the  
2 patients regarding age or gender and between aneurysms regarding their rupture status, neck width,  
3 aneurysm volume, or packing density (table 1). There was a non-significant tendency for a lower packing  
4 density in the recurrent group compared to the non-recurrent group.  
5  
6  
7  
8  
9

### 10 *WSS measurements*

11  
12  
13 The results of the WSS measurements compared between the recurrent and the non-recurrent cohort can be  
14 found in table 2.  
15  
16  
17

18 Neither the absolute nor the normalized values of maximum and spatially averaged WSS at the aneurysm  
19 neck area differed between the two groups. All aneurysms showed some degree of abnormal WSS at the  
20 aneurysm neck. The percentage of the aneurysm neck area that was exposed to abnormal WSS was  
21 significantly higher in the recurrent group compared to the non-recurrent group (Median 49.3% vs. 34.7%;  
22 p=0.011). Only one non-recurrent aneurysm (case number 18) showed a higher percentage area of abnormal  
23 WSS and only one recurrent aneurysm (case number 6) showed a smaller percentage area of abnormal WSS  
24 than the median of all 18 aneurysms (median 45.6%).  
25  
26  
27  
28  
29  
30  
31  
32  
33  
34

### 35 *ROC-curve analysis*

36  
37  
38 In the ROC-curve analysis, the AUC was 0.86 (95% CI 0.62 to 0.98; p< 0.001), the Youden index maximum  
39 value was 0.78 and the percentage of abnormal WSS at that point was 45.1%. Applying this as a threshold  
40 value resulted in a sensitivity and specificity of both 88.9% (95% CI 51.8 – 99.7%). Taking the prevalence  
41 observed in the patient collective of 11.1% as a basis, this results in a positive predictive value of 51.0% and  
42 a negative predictive value of 98.4%. The ROC-curve is displayed in Figure 2.  
43  
44  
45  
46  
47  
48  
49

### 50 *Qualitative evaluation*

51  
52  
53 As expected by the definition of WSS, impingement zones of high velocity flow as seen on the stream line  
54 images coincided with areas of high WSS, while areas exposed to slower flow showed low WSS. High WSS  
55 was seen at bifurcation points, at vessel narrowing, and on uneven vessel surfaces. The WSS was lowest on  
56  
57  
58  
59  
60

1 the straight segments of the inflow vessels. Aneurysms with large neck remnants showed more  
2 compartments with slower flow as seen on the stream line images.  
3

4  
5 The distribution of WSS and flow velocities were very similar between recurrent and non-recurrent  
6 aneurysms with areas of high and low WSS as well as regions of fast and slow flow in both groups. No  
7 pattern could be visually identified that coincided with the location of the recurrences. The visual maps of  
8 WSS and velocity vectors of all cases can be found in Figure 3.  
9  
10  
11  
12  
13  
14  
15  
16  
17  
18

## 19 **Discussion:**

20  
21  
22 The main finding of this study is that the necks of recurrent aneurysms are more often exposed to what we  
23 defined as abnormal WSS. While no statistical differences were found between the recurrent and non-  
24 recurrent aneurysms regarding the percentage areas of either low or high WSS as individual parameters, an  
25 increase of the combination of both parameters was associated with recurrence.  
26  
27  
28  
29  
30  
31

32 Literature on the hemodynamic characteristics of recurrent aneurysms is scarce and most published studies  
33 use 3D-RA as imaging modality, despite the more common use of TOF-MRA as the standard follow-up  
34 imaging modality. To the best of our knowledge, this is the first study to analyze the local blood flow  
35 characteristics in peri-aneurysmal regions by CFD on vessel geometries derived from MRA follow-up data  
36 to compare recurrent and non-recurrent aneurysms.  
37  
38  
39  
40  
41  
42  
43  
44

45 Recently the influence of haemodynamics on the recurrence of cerebral aneurysms has been studied on  
46 larger cohorts of patients. It was found that the inflow rate on basilar tip aneurysms was an predictor of  
47 recurrence after treatment<sup>6</sup> and that changes of the velocity on the neck plane of the aneurysm after  
48 treatment were related to aneurysm recurrence.<sup>23</sup> Fujimura et al. even proposed a combined parameter  
49 combining hemodynamic, morphological, and clinical parameters to predict aneurysm retreatment.<sup>24</sup> In their  
50 study the combined parameter more accurately predicted aneurysm re-treatment than morphological  
51 parameters alone. All these studies performed CFD only on pre-interventional 3D-RA, and either simulated  
52  
53  
54  
55  
56  
57  
58  
59  
60

1 treatment by a porous media method,<sup>25</sup> a virtual stenting technique, subtracted the 3-dimensional geometry  
2 of the coil ball from the pre-interventional images or did not analyze the post-interventional haemodynamics  
3 at all.  
4

5  
6  
7  
8 One research group used pre- and post-treatment 3D-RA datasets to analyze haemodynamics in a small set  
9 of previously totally occluded aneurysms and demonstrated that higher WSS in the neck of the treated  
10 aneurysm was an important hemodynamic factor contributing to aneurysm recurrence.<sup>8,9</sup>  
11  
12

13  
14  
15 The significantly different patterns of WSS between recurrent and non-recurrent aneurysms in our study are  
16 very much in line with what we know about aneurysm growth and rupture in untreated aneurysms: It is  
17 state-of-the-art knowledge that both high and low WSS play an important role in the initiation, growth and  
18 rupture of aneurysms.<sup>26</sup> The physiological basis is that intensified WSS leads to overexpression of Nitric  
19 oxide and, therefore, a non-physiological arterial tone that destroys the endothelium. As the balance between  
20 arterial pressure and internal wall stress forces is disturbed, the vessel wall remodels causing further  
21 degeneration and destruction of the endothelium.<sup>27</sup> In contrast, abnormally low WSS fails to provide the  
22 necessary stimulus for regular function of the endothelium, thus, initiating an apoptotic cell cycle and  
23 leading to degeneration of wall.<sup>2,28</sup> It does not seem far-fetched that the same hemodynamic forces that  
24 influence growth of aneurysms attribute to recurrence too. In our opinion, in coil-embolized aneurysms these  
25 forces do not necessarily act on the embolized volume but on the neck area that is not covered by coils. For  
26 this reason, we included the direct vicinity of the aneurysm neck in our analysis.  
27  
28  
29  
30  
31  
32  
33  
34  
35  
36  
37  
38  
39  
40  
41  
42  
43

44 In our study not only the recurrent but also the non-recurrent aneurysms were subject to abnormal WSS.  
45 This is a result of using the mostly non-bifurcated near vessel segments as a reference to compare to the  
46 mostly bifurcated segments which hold the aneurysms. Alternative definitions of abnormal WSS are a  
47 deviation 10% of the parent vessels mean or one standard deviation of the mean of the near vessel. Both  
48 would have returned some degree of abnormal WSS in all cases. This finding might hinder the use of  
49 abnormal WSS as a prognostic parameter on first sight. On the other hand, we submit that not the mere  
50 presence of any amount of abnormal WSS would lead to aneurysm recurrence, but the area affected has to  
51 pass a certain threshold. Testing our hypothesis, we were able to identify a threshold value of abnormal  
52  
53  
54  
55  
56  
57  
58  
59  
60

1 WSS separating the recurrent and non-recurrent group with only one case falsely classified. This threshold  
2 might be specific to our data and our methodology. Prospective studies are needed to evaluate if abnormal  
3 WSS can be used as a metric to identify recurrent aneurysms a priori. Furthermore, other hemodynamic  
4 indices must be tested for their utility in the prediction of aneurysm recurrence. Pressure indices in particular  
5 are promising candidates as the pressure acting on the coil mass could lead to progressive coil compaction  
6 and subsequently aneurysm recurrence.  
7  
8  
9  
10  
11  
12

13  
14  
15 In qualitative evaluation the locations of the recurrences do not appear visually different to other locations at  
16 the aneurysm neck. Neither did we see a pattern that would have allowed to visually distinguish recurrent  
17 and non-recurrent aneurysms. It has been questioned, however, if visual assessment of color-coded maps of  
18 WSS and flow vectors is useful in the clinical setting, and for this reason CFD sometimes has been  
19 ironically called “Colors For Doctors”.<sup>29</sup>  
20  
21  
22  
23  
24  
25  
26

27 In untreated intracranial aneurysms WSS does not show strong correlations with common geometrical  
28 metrics such as volume, aspect ratio, size ratio and parent vessel diameter.<sup>30</sup> Still, there are geometric  
29 correlates to areas of abnormal WSS in coil-embolized aneurysms. In neck remnants that form nooks for  
30 example blood flow may be slowed down resulting in low WSS. Uneven surfaces at the aneurysm neck may  
31 be subject to increased WSS as well. Coil-embolized aneurysms with large neck remnants would show a  
32 high percentage of abnormal WSS; however, CFD is not necessary to identify these aneurysms as suffering  
33 from a higher risk of recurrence. In treated aneurysms with only small neck remnants on the other hand CFD  
34 has the potential to provide a metric complimentary to morphological parameters alone. We demonstrated  
35 that the application of CFD using 3D TOF-MRA is feasible even in coil-embolized aneurysms. However,  
36 during a pre-testing of the methodology simulations were subject to non-convergence in a sample of three  
37 ICA geometries that by nature have higher flow rates of usually over 200mL/min. Higher blood flow  
38 velocities result in higher Reynolds numbers and as the Reynolds number increases, it becomes less likely  
39 that a stable steady-state solution exists for the simulation. While the input is steady, the flow in the vessels  
40 might then oscillate between two distinct flow patterns, therefore, being unsteady and preventing  
41 convergence of simulations.<sup>31</sup> Valen-Sendstad et al. found that in their study three out of five ICA  
42  
43  
44  
45  
46  
47  
48  
49  
50  
51  
52  
53  
54  
55  
56  
57  
58  
59  
60

1 geometries we subject to periodic and high frequency flow instabilities and only in two geometries flow was  
2 laminar.<sup>32</sup> This problem is well known and can be addressed by extending the entrance region by an artificial  
3 tube to reach a fully developed laminar flow in the petrous section. Nevertheless, we choose to exclude all  
4 ICA aneurysms from this study rather than to artificially alter our geometries.  
5  
6  
7  
8  
9

10 A limitation to this study is the use of follow-up imaging 6 months after treatment. At this point, the  
11 aneurysms possibly already exhibited a recurrence that might not be the result but the cause of altered  
12 haemodynamics. To solve this problem a prospective longitudinal study will be necessary that applies CFD  
13 3D TOF-MRA acquired directly after treatment. Still, even later after treatment the prediction of a continued  
14 growth of a recurrence is useful. A prospective study using imaging datasets acquired directly after  
15 treatment is needed to challenge our findings. Another limitation is the use of 3D TOF-MRA for the  
16 reconstruction of vessel geometries. Compared to 3D-RA, it leads to more uneven vessel geometries and  
17 artefacts may obscure branching vessels. The disadvantage of 3D-RA is that it is not regularly used as  
18 standard follow-up imaging technique. If CFD should be of any clinical use in the follow-up of coil  
19 embolized aneurysms, it would have to be performed on 3D TOF-MRA, which has been shown to  
20 adequately reproduce aneurysm geometry and allow meaningful CFD analysis.<sup>33</sup> Furthermore, the use of  
21 population averaged values of blood flow for the simulations rather than patient individual data may have  
22 led to errors in WSS measurements.<sup>34</sup> To tackle this issue, relative rather than absolute indices were used,  
23 which have been reported as being more comparable in the light of inaccuracies in flow velocities.<sup>1</sup>  
24  
25  
26  
27  
28  
29  
30  
31  
32  
33  
34  
35  
36  
37  
38  
39  
40  
41

42 Additionally, the manual definition of the vicinity of the aneurysm neck might introduce uncertainty into the  
43 data. For our study we assumed that aneurysm growth mediated by WSS at the neck was the reason for the  
44 recanalization and the aneurysm neck was necessarily broadly defined. But Aaneurysm recurrence might as  
45 well result from coil compaction or from aneurysm growthcoil compaction, facilitated by hemodynamic  
46 forces acting either on the coil itself or at aneurysm neck not covered by coil materialon the coil ball itself.<sup>35</sup>  
47 There, coil compaction will rather be caused by pressure. Recently, Nambu et al. found the pressure at a  
48 virtual coil plane compared to and normalized for the proximal vessel to be the strongest predictor for  
49 recurrence after endovascular treatment of ICA aneurysms.<sup>36</sup> To account for both etiologies the vicinity of  
50 the aneurysm neck was necessarily broadly defined. TheOur data might have shown more pronounced  
51  
52  
53  
54  
55  
56  
57  
58  
59  
60

1 differences if the pressure at the coil ball had been analyzed as well and the WSS measurements had been  
2 limited to more discrete areas around the aneurysm neck. Furthermore, we were unable to perfectly match  
3 recurrent with non-recurrent aneurysms resulting in a non-significant tendency towards a lower packing  
4 density in the recurrent group. While these differences itself might have predisposed them for recurrences<sup>37</sup>  
5 we did not see this effect in our sample that had a wide span of packing densities in both cohorts. Lastly, this  
6 study suffered of a small sample size, which might limit the reproducibility of some of the findings of  
7 previous studies or separate the influence of either low or high WSS.  
8  
9  
10  
11  
12  
13  
14  
15  
16

17 Understanding the influence of hemodynamic forces on aneurysm initiation, growth, rupture, and recurrence  
18 after treatment can help to improve therapies and predict outcome. Recurrences of intracranial aneurysms  
19 can already be detected on 3D TOF-MRA with a high accuracy compared to DSA with volumetric  
20 measurements being significantly more reliable than visual inspection.<sup>16, 38</sup> CFD, therefore, might not be  
21 necessary to detect those recurrences. But it may one day guide us to ways to prevent post-treatment  
22 recurrences, test the efficacy of new treatments, and refine follow-up protocols. With the still exponential  
23 increase in computational processing power as described by Moore's law,<sup>39</sup> instantaneous CFD at the time  
24 of follow-up imaging may be possible in the foreseeable future. Less invasive imaging methods than DSA,  
25 still carrying its high resolution and accuracy with the additional benefit of delivering flow information on a  
26 molecular level like the magnetic particle imaging<sup>40</sup> may become available and add to the accuracy of CFD  
27 simulations. CFD simulations still face several hurdles before they are of direct clinical use, but its  
28 importance is only likely to grow in the future.  
29  
30  
31  
32  
33  
34  
35  
36  
37  
38  
39  
40  
41  
42  
43  
44

## 45 *Conclusion*

46 In conclusion, the percentage of abnormal WSS at the aneurysm neck differs between recurrent aneurysms  
47 and non-recurrent aneurysms. Therefore, CFD bears the potential to help identifying patients that would  
48 require closer follow-up or even retreatment and those for whom FU imaging is unnecessary. It needs to be  
49 tested if this hemodynamic biomarker can detect recurrences in a prospectively.  
50  
51  
52  
53  
54  
55  
56  
57  
58  
59  
60

## References:

1. Xiang J, Natarajan SK, Tremmel M, et al. Hemodynamic-morphologic discriminants for intracranial aneurysm rupture. *Stroke* 2011;42:144-52.
2. Shojima M, Oshima M, Takagi K, et al. Magnitude and role of wall shear stress on cerebral aneurysm: Computational fluid dynamic study of 20 middle cerebral artery aneurysms. *Stroke* 2004;35:2500-5.
3. Cebal JR, Mut F, Weir J, Putman C. Quantitative characterization of the hemodynamic environment in ruptured and unruptured brain aneurysms. *AJNR Am J Neuroradiol* 2011;32:145-51.
4. Jou LD, Lee DH, Morsi H, Mawad ME. Wall shear stress on ruptured and unruptured intracranial aneurysms at the internal carotid artery. *AJNR Am J Neuroradiol* 2008;29:1761-7.
5. Watanabe T, Isoda H, Takehara Y, et al. Hemodynamic vascular biomarkers for initiation of paraclinoid internal carotid artery aneurysms using patient-specific computational fluid dynamic simulation based on magnetic resonance imaging. *Neuroradiology* 2018;60:545-55.
6. Sugiyama S, Niizuma K, Sato K, et al. Blood flow into basilar tip aneurysms: A predictor for recanalization after coil embolization. *Stroke* 2016;47:2541-7.
7. Kono K, Terada T. Flow visualization of recurrent aneurysms after coil embolization by 3d phase-contrast mri. *Acta Neurochir (Wien)* 2014;156:2035-40.
8. Luo B, Yang X, Wang S, et al. High shear stress and flow velocity in partially occluded aneurysms prone to recanalization. *Stroke* 2011;42:745-53.
9. Li C, Wang S, Chen J, et al. Influence of hemodynamics on recanalization of totally occluded intracranial aneurysms: A patient-specific computational fluid dynamic simulation study. *J Neurosurg* 2012;117:276-83.
10. Irie K, Anzai H, Kojima M, et al. Computational fluid dynamic analysis following recurrence of cerebral aneurysm after coil embolization. *Asian J Neurosurg* 2012;7:109-15.
11. Cebal J, Mut F, Sforza D, et al. Clinical application of image-based cfd for cerebral aneurysms. *Int j numer method biomed eng* 2011;27:977-92.
12. Bakker NA, Westerlaan HE, Metzemaekers JD, et al. Feasibility of magnetic resonance angiography (mra) follow-up as the primary imaging modality after coiling of intracranial aneurysms. *Acta Radiol* 2010;51:226-32.
13. Buhk JH, Kallenberg K, Mohr A, Dechent P, Knauth M. Evaluation of angiographic computed tomography in the follow-up after endovascular treatment of cerebral aneurysms--a comparative study with dsa and tof-mra. *Eur Radiol* 2009;19:430-6.
14. Park JH, Kang HS, Han MH, Jeon P, Yoo DS, Lee TH. Embolization of intracranial aneurysms with hydrosoft coils: Results of the korean multicenter study. *AJNR Am J Neuroradiol*;32:1756-61.
15. Youn SW, Cha SH, Kang HS, Cho YD, Han MH. Matrix(2) coils in embolization of intracranial aneurysms: 1-year outcome and comparison with bare platinum coil group in a single institution. *AJNR Am J Neuroradiol* 2011;32:1745-50.
16. Schonfeld MH, Schlotfeldt V, Forkert ND, et al. Aneurysm recurrence volumetry is more sensitive than visual evaluation of aneurysm recurrences. *Clin Neuroradiol* 2016;26:57-64.
17. Reymond P, Bohraus Y, Perren F, Lazeyras F, Stergiopoulos N. Validation of a patient-specific one-dimensional model of the systemic arterial tree. *Am J Physiol Heart Circ Physiol* 2011;301:H1173-82.
18. Peach T, Spranger K, Ventikos Y. Virtual flow-diverter treatment planning: The effect of device placement on bifurcation aneurysm haemodynamics. *Proc Inst Mech Eng H* 2017;231:432-43.
19. Retarekar R, Ramachandran M, Berkowitz B, et al. Stratification of a population of intracranial aneurysms using blood flow metrics. *Comput Methods Biomech Biomed Engin* 2015;18:1072-82.
20. Zarrinkoob L, Ambarki K, Wahlin A, Birgander R, Eklund A, Malm J. Blood flow distribution in cerebral arteries. *J Cereb Blood Flow Metab* 2015;35:648-54.
21. Dempere-Marco L, Oubel E, Castro M, Putman C, Frangi A, Cebal J. Cfd analysis incorporating the influence of wall motion: Application to intracranial aneurysms. *Med Image Comput Comput Assist Interv* 2006;9:438-45.
22. Richards A. University of oxford advanced research computing. 2015. In: Zenodo. Available at: <http://doi.org/10.5281/zenodo.22558>. Accessed January 24, 2019.
23. Zhang Q, Jing L, Liu J, et al. Predisposing factors for recanalization of cerebral aneurysms after endovascular embolization: A multivariate study. *J Neurointerv Surg* 2018;10:252-7.
24. Fujimura S, Takao H, Suzuki T, et al. A new combined parameter predicts re-treatment for coil-embolized aneurysms: A computational fluid dynamics multivariable analysis study. *J Neurointerv Surg* 2018;10:791-6.

- 1 25. Mitsos AP, Kakalis NM, Ventikos YP, Byrne JV. Haemodynamic simulation of aneurysm coiling in an  
2 anatomically accurate computational fluid dynamics model: Technical note. *Neuroradiology* 2008;50:341-7.
- 3 26. Berge J, Blanco P, Rooryck C, et al. Understanding flow patterns and inflammatory status in intracranial  
4 aneurysms: Towards a personalized medicine. *J Neuroradiol* 2016;43:141-7.
- 5 27. Sforza DM, Putman CM, Cebal JR. Hemodynamics of cerebral aneurysms. *Annu Rev Fluid Mech* 2009;41:91-  
6 107.
- 7 28. Malek AM, Alper SL, Izumo S. Hemodynamic shear stress and its role in atherosclerosis. *JAMA*  
8 1999;282:2035-42.
- 9 29. Steinman DA. Computational modeling and flow diverters: A teaching moment. *AJNR Am J Neuroradiol*  
10 2011;32:981-3.
- 11 30. Evju O, Valen-Sendstad K, Mardal KA. A study of wall shear stress in 12 aneurysms with respect to different  
12 viscosity models and flow conditions. *J Biomech* 2013;46:2802-8.
- 13 31. Baek H, Jayaraman MV, Richardson PD, Karniadakis GE. Flow instability and wall shear stress variation in  
14 intracranial aneurysms. *J R Soc Interface* 2010;7:967-88.
- 15 32. Valen-Sendstad K, Piccinelli M, Steinman DA. High-resolution computational fluid dynamics detects flow  
16 instabilities in the carotid siphon: Implications for aneurysm initiation and rupture? *J Biomech* 2014;47:3210-6.
- 17 33. Goubergrits L, Schaller J, Kertzscher U, Petz C, Hege HC, Spuler A. Reproducibility of image-based analysis of  
18 cerebral aneurysm geometry and hemodynamics: An in-vitro study of magnetic resonance imaging, computed  
19 tomography, and three-dimensional rotational angiography. *J Neurol Surg A Cent Eur Neurosurg* 2013;74:294-302.
- 20 34. Mynard JP, Wasserman BA, Steinman DA. Errors in the estimation of wall shear stress by maximum doppler  
21 velocity. *Atherosclerosis* 2013;227:259-66.
- 22 35. Abdihalim M, Watanabe M, Chaudhry SA, Jagadeesan B, Suri MF, Qureshi AI. Are coil compaction and  
23 aneurysmal growth two distinct etiologies leading to recurrence following endovascular treatment of intracranial  
24 aneurysm? *J Neuroimaging* 2014;24:171-5.
- 25 36. Nambu I, Misaki K, Uchiyama N, et al. High pressure in virtual postcoiling model is a predictor of internal  
26 carotid artery aneurysm recurrence after coiling. *Neurosurgery* 2019;84:607-15.
- 27 37. Tamatani S, Ito Y, Abe H, Koike T, Takeuchi S, Tanaka R. Evaluation of the stability of aneurysms after  
28 embolization using detachable coils: Correlation between stability of aneurysms and embolized volume of  
29 aneurysms. *AJNR Am J Neuroradiol* 2002;23:762-7.
- 30 38. van Amerongen MJ, Boogaarts HD, de Vries J, et al. Mra versus dsa for follow-up of coiled intracranial  
31 aneurysms: A meta-analysis. *AJNR Am J Neuroradiol* 2014;35:1655-61.
- 32 39. Vosburgh KG, Newbower RS. Moore's law, disruptive technologies, and the clinician. *Stud Health Technol*  
33 *Inform* 2002;85:8-13.
- 34 40. Haegele J, Sattel T, Erbe M, et al. [magnetic particle imaging (mpi)]. *Rofo* 2012;184:420-6.
- 35
- 36
- 37
- 38
- 39
- 40
- 41
- 42
- 43
- 44
- 45
- 46
- 47
- 48
- 49
- 50
- 51
- 52
- 53
- 54
- 55
- 56
- 57
- 58
- 59
- 60

**Table 1: Population characteristics in the recurrent and non-recurrent cohort**

Parameter	Recurrence (n=9)	No recurrence (n=9)	p value
Age [years]**	70 (53-76)	61 (33-75)	.400
Female, [n] (%)	5 (55.6)	7 (77.8)	.620
Ruptured aneurysms, [n] (%)	0 (0)	3 (33.3)	.206
Neck width [mm]*	5.3 ± 1.9	4.3 ± 0.8	.152
Aneurysm volume [μl]*	180.8 ± 160.0	88.3 ± 75.3	.161
Packing density [%]*	27.8 ± 5.3	34.2 ± 7.8	.071

\* Data are means ± standard deviations.

\*\* Data are medians (range).

n = number

Peer Review

**Table 2: Results of wall shear stress measurements in the recurrent and the non-recurrent cohort in the aneurysm neck area**

Parameter	Recurrence (n=9)	No recurrence (n=9)	p value
Maximal WSS [Pa]*	49.3 ± 22.5	42.4 ± 18.7	.516
Normalized Maximal WSS*	0.9 ± 0.3	1.0 ± 0.4	.744
Mean WSS [Pa]*	7.2 ± 5.3	8.3 ± 1.5	.540
Normalized Mean WSS*	1.4 ± 0.6	1.33 ± 0.2	.702
Abnormal WSS area [%]**	49.3 (5.9)	34.7 (17.0)	.011 †
High WSS area [%]**	30.7 (31.2)	25.0 (9.5)	.436
Low WSS area [%]**	14.4 (30.8)	9.7 (11.7)	.340

\* Data are means ± standard deviations.

\*\* Data are medians (interquartile range).

† significance (p<0.05)

n = number

Review

1  
2  
3  
4 **Figure legends:**  
5  
6  
7

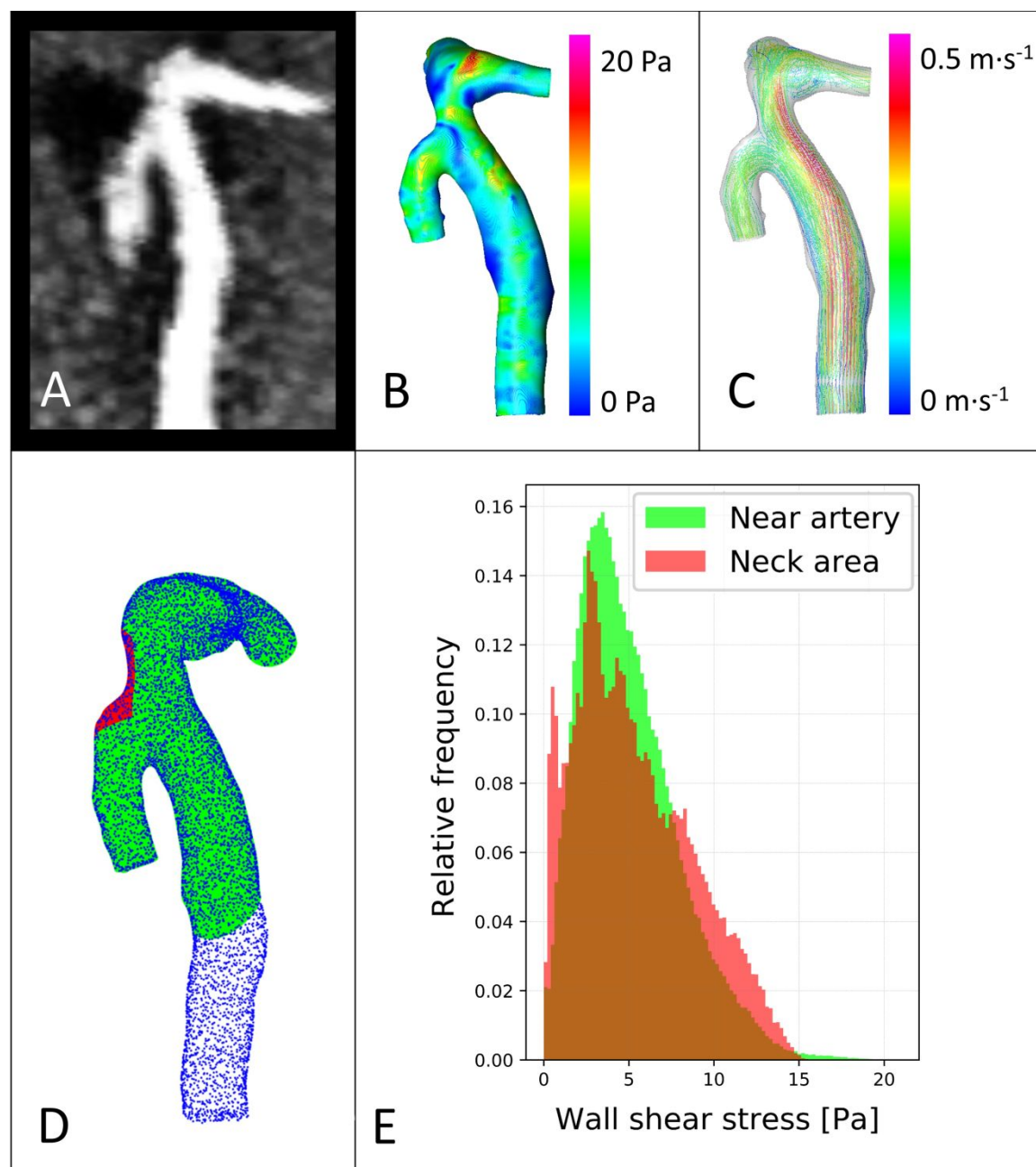


**Fig.1** Case of a non-recurrent middle cerebral artery aneurysm. From the 3D TOF-MRA source images 6 months after intervention (A) a geometry was constructed. Wall shear stress (WSS) was plotted color scaled between 0 Pa and 20 Pa to the vessel surface (B) and streamlines were visualized according to the flow velocity color scaled between 0 m·s<sup>-1</sup> and 0.5 m·s<sup>-1</sup> (C). Summary statistics of WSS were calculated at the

1 neck area (red) and the near artery (green) (D). A corresponding histogram (E) shows the uneven  
2 distribution of WSS at the neck area (red) compared to the near vessel (green).  
3  
4  
5  
6  
7  
8  
9  
10  
11  
12  
13  
14  
15  
16  
17  
18  
19  
20  
21  
22  
23  
24  
25  
26  
27  
28  
29  
30  
31  
32  
33  
34  
35  
36  
37  
38  
39  
40  
41  
42  
43  
44  
45  
46  
47  
48  
49  
50  
51  
52  
53  
54  
55  
56  
57  
58  
59  
60

For Peer Review

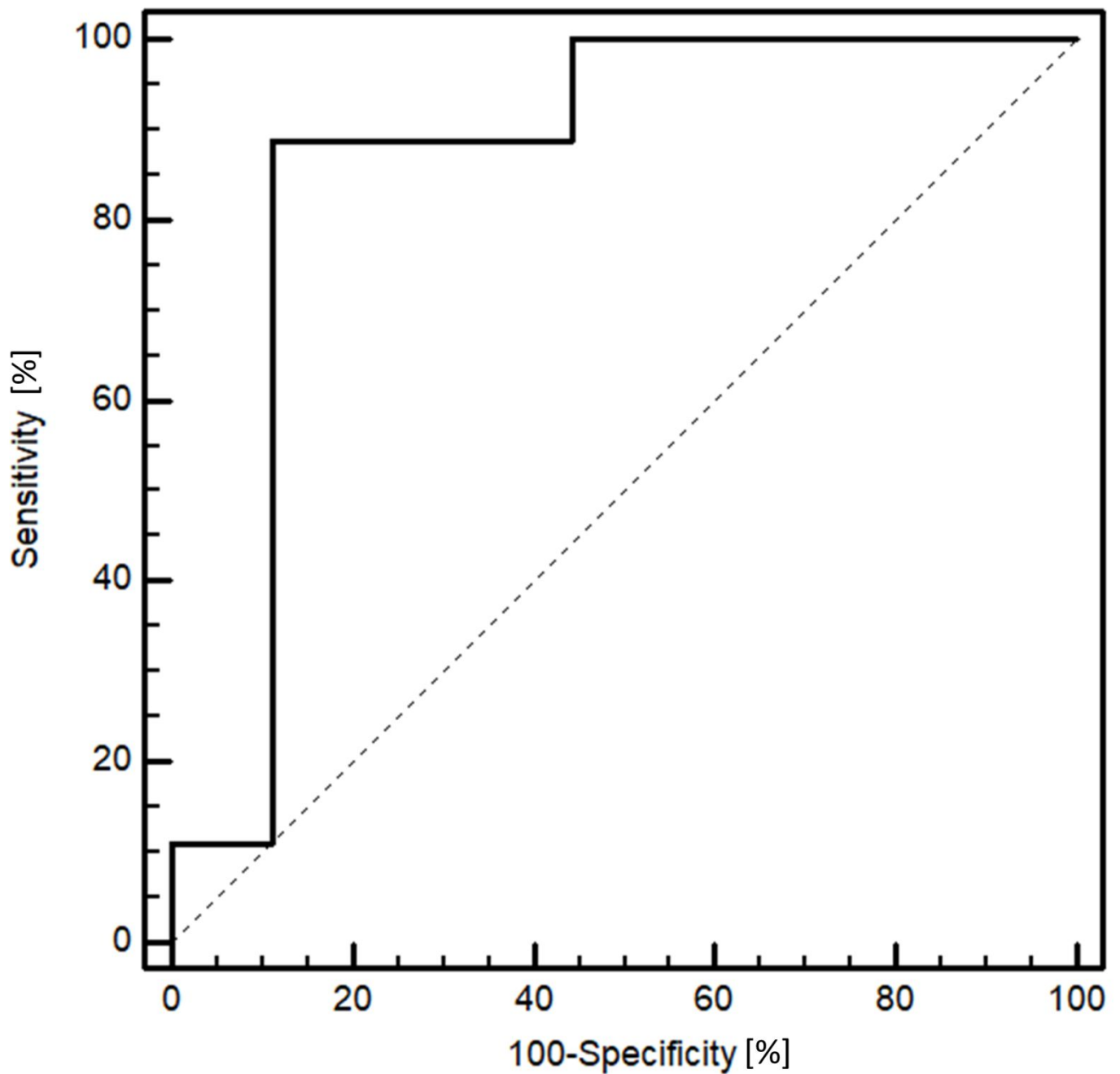


**Fig.2** Receiver operating characteristic curve plotting the true positive rate (Sensitivity)[%] in function of the false positive rate (100-Specificity)[%] for different cut-off points of the percentage of the neck area exposed to abnormal wall shear stress in recurrent versus non-recurrent aneurysms.

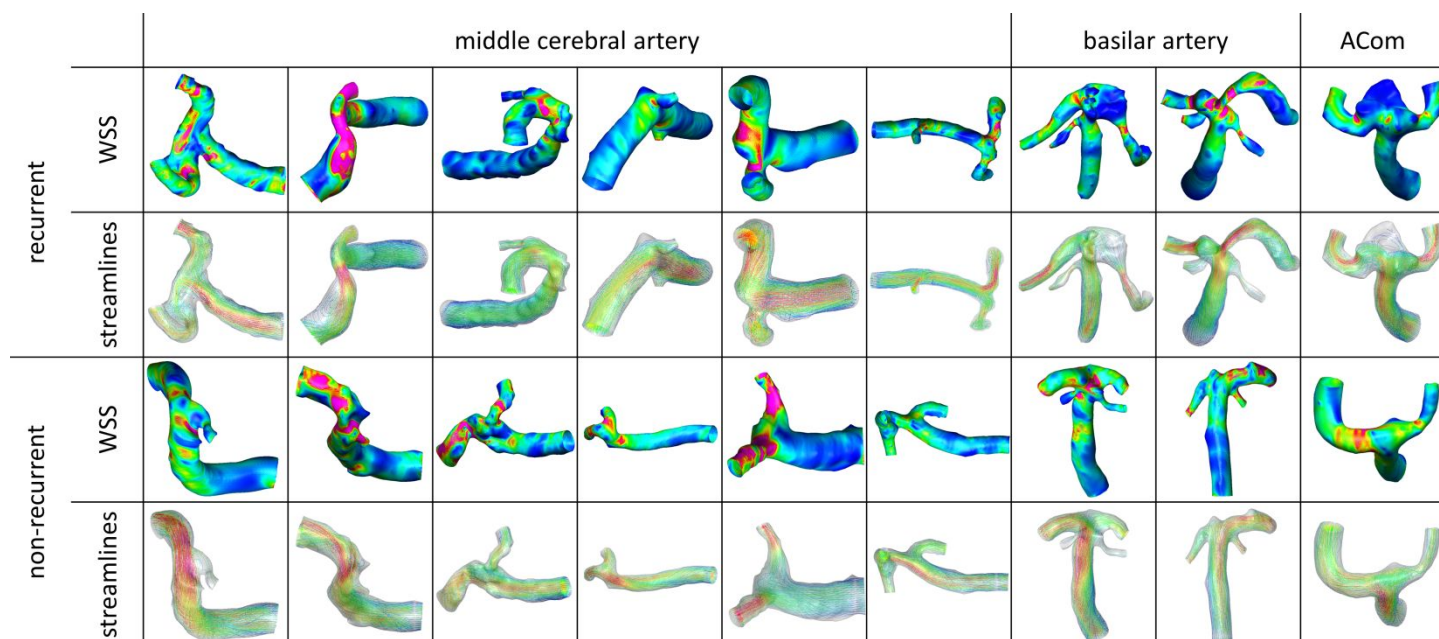


**Fig.3** Compilation showing the recurrent (upper two rows) compared to the non-recurrent cases (lower two rows) of middle cerebral artery, basilar artery and anterior communicating artery (ACom) aneurysms. Wall shear stress (WSS) was plotted color scaled between 0 Pa and 20 Pa to the vessel surface (first and third row) and streamlines were visualized according to the flow velocity color scaled between 0 m·s<sup>-1</sup> and 0.5 (second and fourth row).

1  
2  
3  
4  
5  
6  
7  
8  
9  
10  
11  
12  
13  
14  
15  
16  
17  
18  
19  
20  
21  
22  
23  
24  
25  
26  
27  
28  
29  
30  
31  
32  
33  
34  
35  
36  
37  
38  
39  
40  
41  
42  
43  
44  
45  
46  
47  
48  
49  
50  
51  
52  
53  
54  
55  
56  
57  
58  
59  
60

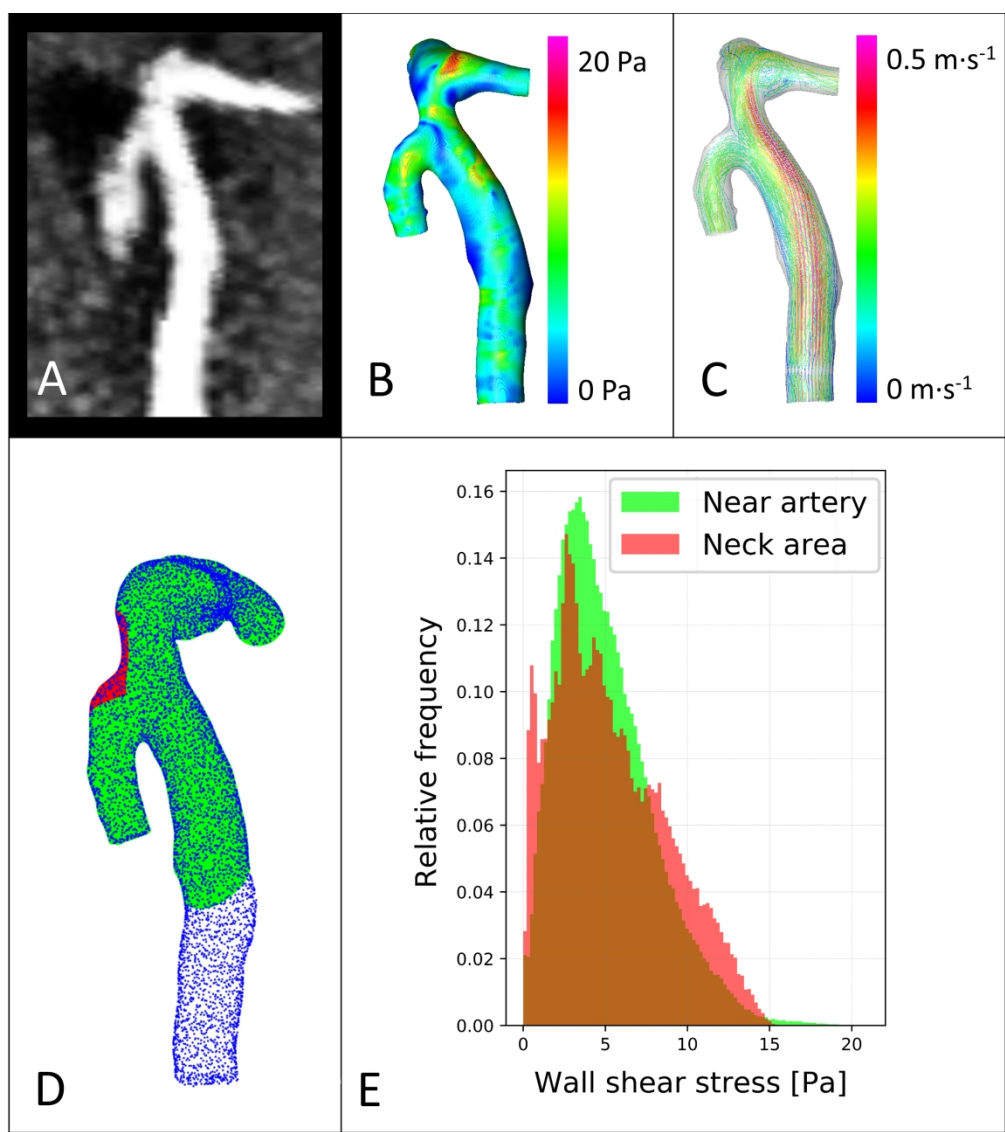


Fig.1 Case of a non-recurrent middle cerebral artery aneurysm. From the 3D TOF-MRA source images 6 months after intervention (A) a geometry was constructed. Wall shear stress (WSS) was plotted color scaled between 0 Pa and 20 Pa to the vessel surface (B) and streamlines were visualized according to the flow velocity color scaled between 0 m·s<sup>-1</sup> and 0.5 m·s<sup>-1</sup> (C). Summary statistics of WSS were calculated at the neck area (red) and the near artery (green) (D). A corresponding histogram (E) shows the uneven distribution of WSS at the neck area (red) compared to the near vessel (green).

267x299mm (300 x 300 DPI)

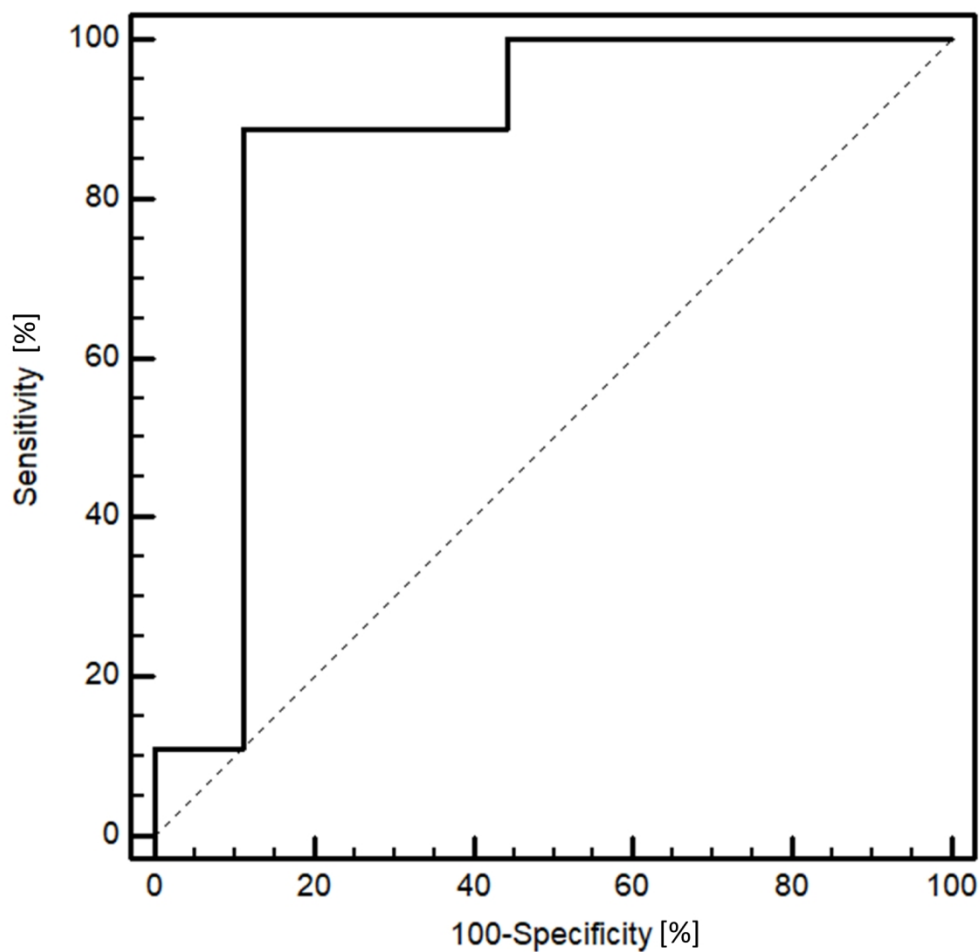


Fig.2 Receiver operating characteristic curve plotting the true positive rate (Sensitivity)[%] in function of the false positive rate (100-Specificity)[%] for different cut-off points of the percentage of the neck area exposed to abnormal wall shear stress in recurrent versus non-recurrent aneurysms.

476x481mm (96 x 96 DPI)

1  
2  
3  
4  
5  
6  
7  
8  
9  
10  
11  
12  
13  
14  
15  
16  
17  
18  
19  
20  
21  
22  
23  
24  
25  
26  
27  
28  
29  
30  
31  
32  
33  
34  
35  
36  
37  
38  
39  
40  
41  
42  
43  
44  
45  
46  
47  
48  
49  
50  
51  
52  
53  
54  
55  
56  
57  
58  
59  
60

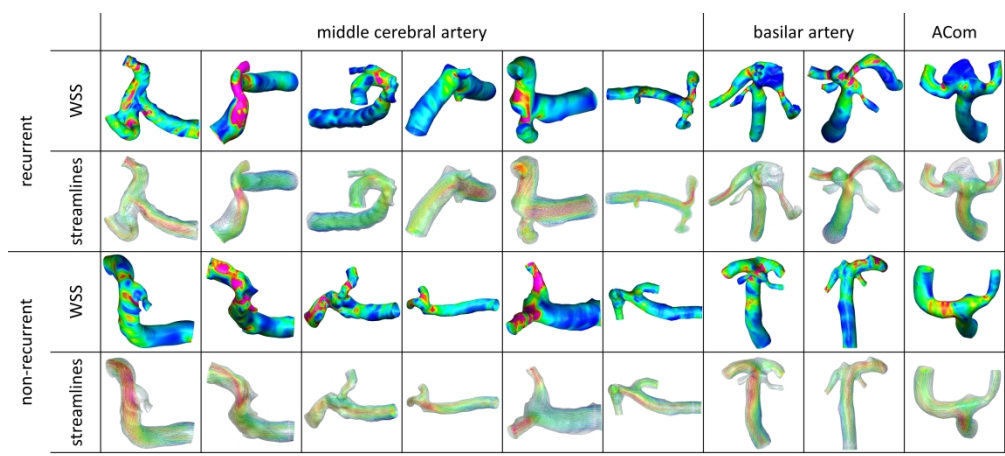


Fig.3 Compilation showing the recurrent (upper two rows) compared to the non-recurrent cases (lower two rows) of middle cerebral artery, basilar artery and anterior communicating artery (ACom) aneurysms. Wall shear stress (WSS) was plotted color scaled between 0 Pa and 20 Pa to the vessel surface (first and third row) and streamlines were visualized according to the flow velocity color scaled between 0 m·s<sup>-1</sup> and 0.5 (second and fourth row).

1167x515mm (96 x 96 DPI)